Z. Physik B - Condensed Matter 38, 191-199 (1980)

Condensed Matter
Zeitschrift für Physik B

I. XPS Study of 3*d*-Metal Ions Dissolved in Aluminium

P. Steiner, H. Höchst*, W. Steffen, and S. Hüfner
Fachbereich Physik der Universität des Saarlandes, Saarbrücken, Federal Republic of Germany

Received February 22, 1980

The core and valence band spectra of dilute AlMn, AlNi and AlCu alloys have been investigated by x-ray induced photoemission spectroscopy (XPS). The 2*p* levels of Mn and Cu in AlMn and AlCu change only slightly compared to their properties in the pure metals, whereas those of Ni in AlNi lose both their asymmetry and the two hole satellite. The 3*s* spectra of Mn in AlMn show a splitting of 2.9 eV, as compared to 4.3 eV in Mn metal. This indicates that in AlMn the Mn ion is magnetic, at least in the time scale of the XPS measurement. The valence band spectra of the alloys (and of AlFe and AlCo) show virtual bound states with a width of about 1.5 eV and a distance relative to the Fermi energy which increases with increasing *d*-occupancy. The energy of the Al plasmons increase with increasing *d*-metal content.

I. Introduction

The investigation of transition metal impurities in simple metals is interesting in its own right but also as one of the steps for an understanding of the band structure of the metals themselves. The state of a *d*-electron in a *s-p*-band metal is generally described by the Friedel-Anderson virtual bound state (vbs) model [1, 2] which treats the *d*-orbital in the Hartree-Fock approximation as sitting in the *s-p* conduction band. This model has been contested by Hirst [3], who suggested the use of an approach for *d*-metal impurities which has generally been thought to be applicable only to 4*f* elements. This approximation constructs first the ionic groundstate and then places it into the conduction band. At present it is difficult to decide on the basis of the experimental material available, which model represents the situation correctly.

In the case of nonmagnetic impurities (eg. AlCu) both approaches lead to the same electronic energy level schemes, namely an impurity resonance in the *s-p* conduction band. In the magnetic case, however, the Anderson model [2] would predict an exchange split doublet, whereas the Hirst model [3] would predict one or more Hunds rule states, split by a crystal field and broadened by the interaction with the conduction electrons.

The situation is complicated by the following fact: *d*-electron ions in *s-p* band metals (simple metals) are rarely magnetic [4, 5] and due to problems of their preparation and handling have not received very large attention from experimentalists. The "classical" impurity systems - like e.g. CuFe, CuMn, AuFe etc., to name only a few - which have generally been used to test theoretical predictions, should, however, be viewed with some reservation in this respect. Although it is generally argued, that these materials accurately correspond to the theoretical models of a *d*-metal in a *s-p*-band host metal, one has to notice, that in reality an open *d*-metal ion is sitting in a closed shell-*d*-metal band. It is not obvious whether it is reasonable to neglect the closed *d*-shell of the host altogether. In fact recent cluster calculations by Johnson et al. [6] do at least indicate, that there is a large hybridization between the impurity and the host *d*-electron states which influences the energy level scheme of systems like CuFe strongly.

Our laboratory has had a standing interest [7] in the electronic structure of the systems characterized above. The bulk of the data accumulated so far by electron spectroscopy on systems like CuFe can possibly be interpreted [8] in the frame of the calculations of Johnson et al. [6]. It would be premature, however, to state that they prove them. It was therefore decided to publish some of the material obtained so far. In this communication, we shall start with the

* Present address: Max-Planck-Institut für Festkörperforschung, D-7000 Stuttgart 80, Federal Republic of Germany

0340-224X/80/0038/0191/$01.80

simple systems AlMn, AlNi and AlCu together with our earlier data on AlFe and AlCo [7] which can be viewed as models for *d*-electrons in a *s-p* conduction band. Of these alloys AlMn is generally viewed as a spin fluctuation system whereas the other are nonmagnetic alloys [4]. In nonmagnetic alloys the vbs picture has found wide verification by optical data [5, 9, 10] and by direct electron spectroscopy [7, 11, 12], especially in the situation where the host metal has a closed *d*-shell, (e.g. AgPd). Here the *d*-resonance is found sitting in the *s-p*-band, showing a Lorentzian shape, with only minor modifications in the host *d*-band visible.
Optical data of AlMn and AlCu alloys have been published by Beaglehole and Wihl [9] and comparison with this work will be made at the appropriate places of this paper.

II. Experimental

The spectra were recorded with a modified Hewlett-Packard 5950 A spectrometer. The energy resolution of the instrument is 0.6 eV. The pressure in the instrument was in the low 10^{-11} Torr range. The solid solubility of *d*-metal impurities in aluminium is normally very small. One can, however, produce metastable alloys by coevaporation [9], a method which was employed also in the present investigation. The XPS data show that precipitation must be small because no second phase could be detected in the core level or valence band spectra. The contamination of the samples was monitored by the C 1*s* and O 1*s* line. Measurements were stopped as soon as the O 1*s* line became visible. The concentrations were determined from the Al 2*s* or Al 2*p* spectra and the impurity 2*p* spectra. The intensity ratio of two core lines is given by [13]

$$I_1/I_2=\frac{\sigma_1\cdot\lambda(E_{K_1})\cdot n_1}{\sigma_2\cdot\lambda(E_{K_2})\cdot n_2} \tag{1}$$

where I_1 and I_2 are the intensities of the lines, σ_1 and σ_2 are the differential photoabsorption crossections for Al K_α radiation ($h\omega=1{,}487$ eV); $\lambda(E_{K_1})$, $\lambda(E_{K_2})$ are the escape depths of the electrons emitted with kinetic energies E_{K_1}, E_{K_2}, where the kinetic energies E_K are obtained from the binding energy E of the line by $E_K=h\omega-E$; n_1, n_2 is the number of atoms of the corresponding elements per unit volume of the alloy.
The intensities were determined from the spectra by using the non-divergent Mahan lineshape [14]. The crossections were taken from Scofield [15] and from Reilman et al. [16]. The escape depths were calculated from the relation given by Penn [17]

$$\lambda=\frac{E_K}{a\cdot(\ln(E_K)+b)} \tag{2}$$

where a and b are constants depending only on the sample.
This relation is valid for $E_K>200$ eV and is therefore very well suited for XPS investigations. For most materials the constant b is approximately 2.3. Equation (2) can then be approximated [18] by

$$\lambda=a^*\cdot E_K^{0.71} \tag{3}$$

where a is a new constant, depending only on the sample. Using this we get for the intensity ratio

$$\frac{I_1}{I_2}=\frac{\sigma_1}{\sigma_2}\cdot\left\{\frac{E_{K_1}}{E_{K_2}}\right\}^{0.71}\cdot\frac{n_1}{n_2}. \tag{1'}$$

Of course, Eq. (1') can only be used for the determination of element concentrations in a homogeneous system, and its use may be questionable for Ni because of the very low solubility of Ni in Al [19]. It is also necessary that the energy loss contribution should have the same structure for both XPS lines. This is the case for AlCu, AlNi and AlMn. For AlNi the intensity of the two-hole satellite of the Ni 2*p* lines has also to be taken into account. With these reservations in mind the intensities determined with (1') can at best have an accuracy of about 10 percent and will probably be even less accurate for the case of AlNi.

III. Core Level Spectra

a) AlCu; Cu 2p Lines

XPS spectra of an $AlCu_{0.025}$ alloy are shown in Fig. 1. The fits to the spectra have been obtained as explained in detail in a previous communication [14]. The asymmetry parameter of the Al lines ($\alpha=0.10$) was the same as in pure Al. The plasmons were approximated by two Lorentzians of different height and width in order to simulate the effect of the dispersion on the plasmon lineshape. The parameters obtained from the fit of the Al 2*s* line are in good agreement with those of pure Al, a not unexpected result in view of the low impurity concentration.
The Cu 2*p* spectrum exhibits clearly the Al loss structure accompanying the Cu lines. This loss structure has parameters identical to those obtained from the Al 2*s* lines of this alloy. The asymmetry parameter for the Cu lines is small ($\alpha=0.02$) with the same value as in pure Cu and does not show a dependence on concentration.

b) AlNi, Ni 2p Lines

A Ni 2*p* spectrum of an $AlNi_{0.028}$ alloy is shown in Fig. 2. In this system the situation is less favourable

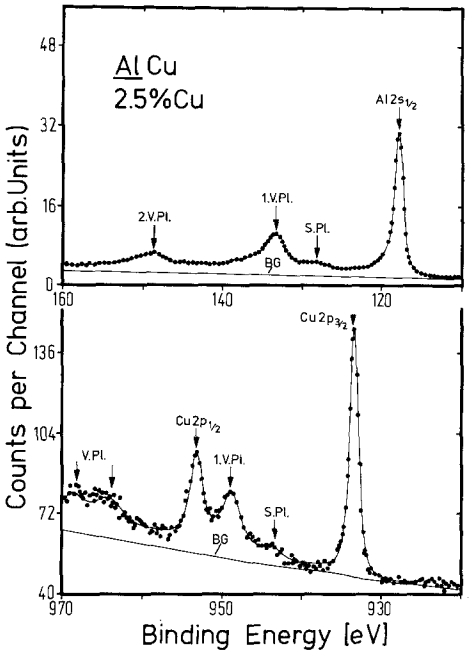

Fig. 1. XPS spectra of the Al 2*s* region and of the Cu 2*p* region of an AlCu alloy. The solid line through the data points is the result of a fit. *BG* is a smooth background. The positions of the volume plasmons (*v.pl.*) and surface plasmons (*s.pl.*) are indicated

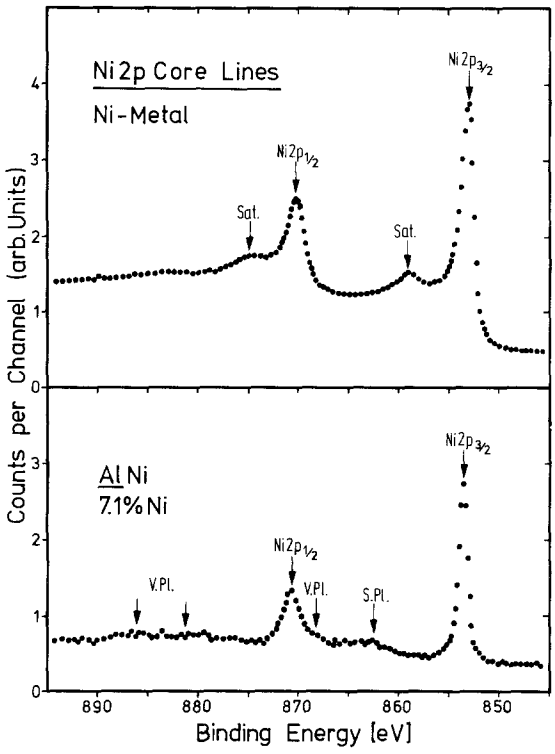

Fig. 3. XPS spectra of the Ni 2*p* region of Ni metal and of an AlNi alloy. The position of the different volume plasmon (*v.pl.*) and surface plasmon (*s.pl.*) lines in AlNi and of the satellite (*Sat.*) lines in Ni metal are indicated

than for the AlCu alloys because the Al volume plasmon accompanying the Ni $2p_{3/2}$ line overlaps strongly the Ni $2p_{1/2}$ line. This makes the evaluation of the data slightly less accurate than for AlCu. The asymmetry parameter for the Ni 2*p* lines ($\alpha = 0.03$) is nearly the same as for the 2*p* lines of Cu in AlCu and shows no dependence on concentration up to 10 percent. This value is much smaller than in pure Ni ($\alpha = 0.22$). The core and valence band spectra of Ni and Ni compounds have received much attention recently

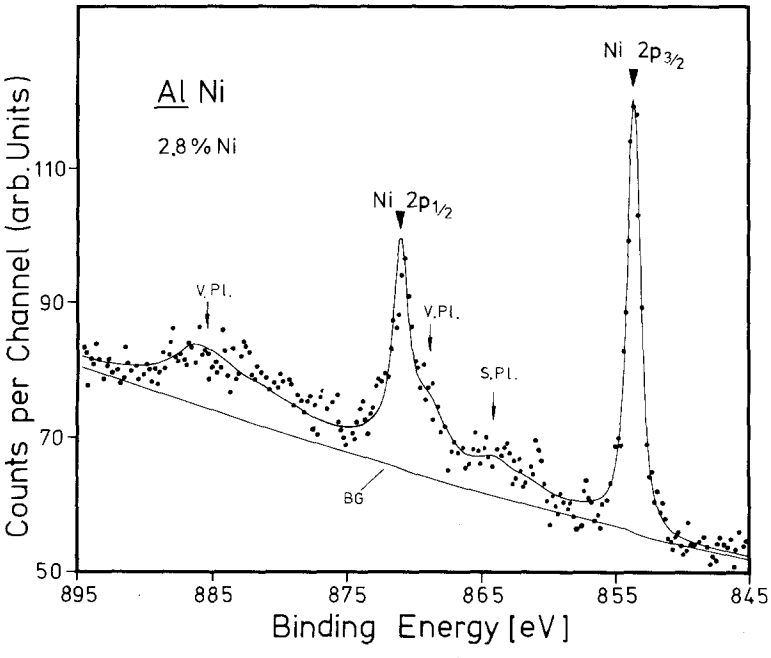

Fig. 2. XPS spectrum of the Ni 2*p* region of an AlNi alloy. The solid line through the data points is the result of a fit. *BG* is a smooth background. The position of the volume plasmons (*v.pl.*) and surface plasmons (*s.pl.*) are indicated

because of some unique features [20–21]. To facilitate the discussion, Fig. 3 shows a Ni $2p$ spectrum of Ni metal and a Ni $2p$ spectrum of a $AlNi_{0.071}$ alloy. These spectra clearly indicate the problem. The Ni metal spectra show a very high background on the high binding energy side and in addition are accompanied by a satellite at about 6 eV to larger binding energies. This satellite is visible in all core levels and also in the valence band and has been the focus of much speculation.

The large background in the spectra of Ni metal can be analyzed with a Mahan lineshape yielding $\alpha = 0.22$. We are of course aware of the fact that this lineshape function only applies rigorously to a free electron metal [22], but it can be used here as a sensible approximation. This means in essence that there is a large probability for low lying electron-hole excitations accompanying the creation of the photohole. Since the density of states of Ni is large at the Fermi energy, this is in accord with this picture, (large α's are also found for Fe, Pd, Pt etc.). The situation in AlNi alloys is very different. Here the Ni d-electrons are sitting in a vbs removed from the Fermi energy (see Fig. 9) and thus the d-density of states is small there. This makes the small α understandable.

The 6 eV satellite clearly visible in the Ni metal spectra is absent in the $AlNi_{0.07}$ spectra (and the $AlNi_{0.028}$ spectrum in Fig. 2. We can not exclude the possibility that there is a small signal at this position, however, it is certainly largely reduced as compared to Ni metal). Satellites are a very common feature in photoelectron spectra – however their intensity relative to the main line varies vastly. In essence these satellites are a consequence of the fact that the electronic states in atoms, molecules and solids, are not one electron states. Therefore in the photoemission process there is always a finite possibility of exciting two electrons instead of one, and the two hole states thus produced are the origin of the satellites – where the main lines are called one hole states in this picture. The explanation of the 6 eV satellites in Ni metal as due to a two hole state was given by Mott [23] and later by Hüfner and Wertheim [20] along the lines of theoretical calculations of Kotani and Toyozawa [24]. It was argued that the strength of the satellite is particularly large in Ni metal, because in this case a second electron is excited into an empty d-state just above the Fermi energy. This view also explains why the strong satellite must be absent in AlNi. In this system the d-states are all filled and far away from the Fermi energy, making the transfer into an empty d-state impossible. It has to be added, that other two electron transitions are possible in AlNi, but are too weak to be observable.

Thus it is concluded from these experiments that the prime requirement for the strong 6 eV satellite to be observable in Ni and its compounds, is the existence of an unoccupied d-state and not the chemical nature of the Ni ion. Therefore the satellite is observed in Ni metal [20] Ni-phtalocyanine [25] and "atomic" Ni [21] – all of which have unoccupied d-states – and can not be seen in AlNi because (as we will show later) it has no empty d-state although the Ni d-states in AlNi are certainly more localized than e.g. in Ni metal, meaning that the degree of localization has little influence on the satellite intensity.

This interpretation is also in agreement with the Fano [26] type resonance enhancement observed recently for the satellites. This means that in experiments employing synchrotron radiation a large intensity enhancement of the satellites is observed if the photon energy is swept through the $3p$ binding energy [21].

It is assumed for the sake of the argument, that Ni is in a $3p^6 3d^9$ configuration in the groundstate. This leads in a photoemission excitation from the d-band to $3p^6 3d^8 d^*$ (main line) and $3p^6 3d^7 d^*$ (satellite line) as the one hole and two hole state respectively, where we have marked the screening electron by a star. The resonance enhancement of the satellite can now occur if the final state $3p^6 3d^7 d^*$ is achieved by a different process:

$$3p^6 d^9 + \hbar\omega \xrightarrow[\text{emission}]{\text{photon}} 3p^5 d^9 d^* \xrightarrow{\text{Auger}} 3p^6 d^7 d^* + e$$

where at resonance the kinetic energy of the electron must be identical to that of a d-electron excited in a two electron excitation leaving behind the $3p^6 3d^7 d^*$ final state. One realizes immediately that this type of process is again very general because the screening electron can also be a s or p-electron, and indeed the resonance enhancement has been observed in Cu-metal and Cu-phtalocyanine [27].

c) *AlMn, Mn 2p Lines*

A spectrum of the Mn $2p$ lines in an $AlMn_{0.12}$ alloy is shown in Fig. 4. Again the Al loss structure accompanying the lines is clearly visible. The fit to the experimental spectrum is not perfect. The asymmetry parameter deduced from the fit is $\alpha = 0.21$, and varies only slightly as a function of the Mn concentration. This value cannot be compared with the one obtained in pure Mn because in that case the lines could not be reproduced by a Mahan lineshape. This is presumably due to the occurrence of complicated final state structure in the spectra of pure Mn due to the unfilled d-shell [28]. Such structure although less

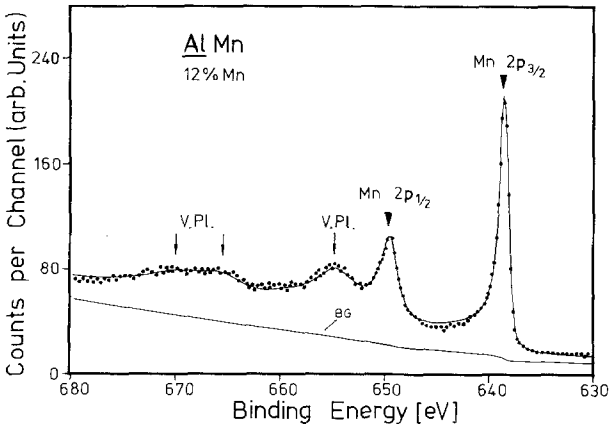

Fig. 4. XPS spectrum of the Mn 2*p* region of an AlMn alloy. The solid line through the data points is the result of a fit. *BG* is a smooth background. The position of the volume plasmons (*v.pl.*) is indicated

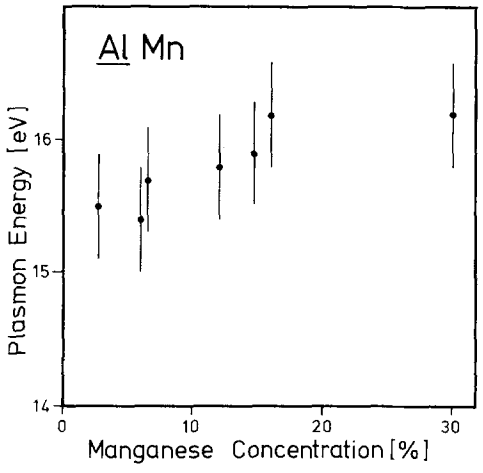

Fig. 5. Plasmon energy of the volume plasmon in AlMn alloys as function of the Mn concentration

important should also be visible in AlMn alloys and it may be the reason for the unsatisfactory fit of the experimental spectrum.

The Mn alloys were investigated over the widest range of impurity concentration and therefore give the most information about the dependence of the plasmon energy on concentration. The results in Fig. 5 show a slight increase in the plasmon energy with increasing Mn concentration. A similar trend has been observed by Beaglehole and Wihl [9] in optical measurements.

d) AlMn, Mn 3s

The *s* lines of open shell ions (*d*- and *f*-ions) show a splitting [28], which is a result of the coupling of the

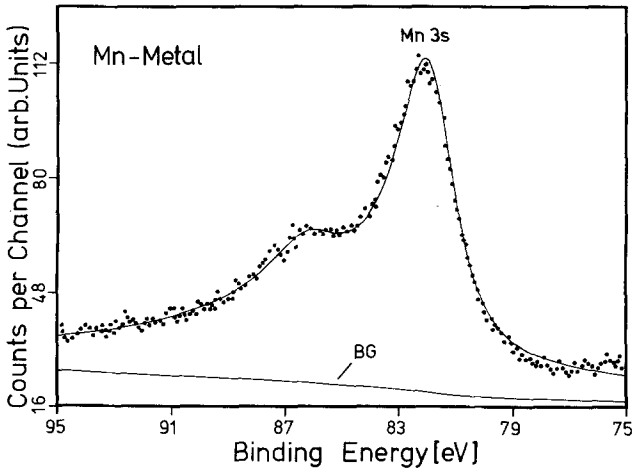

Fig. 6. XPS spectrum of the Mn 3*s* region in Mn metal. The solid line through the data points is the result of a fit. *BG* is a smooth background

spin of the final state photohole to the spin of the open shell. Such splittings are well established and Fig. 6 which shows the 3*s* line of Mn metal, which clearly exhibits a splitting of 4.3 eV, as found also previously by McFeely et al. [29]. This spectrum can also be used to determine the asymmetry parameters and yields $\alpha = 0.24$ - not too different from $\alpha = 0.21$ in AlMn. This indicates that the local electronic environment in the alloy is similar to that in Mn. And in fact the vbs of AlMn intersects the Fermi energy (see Sect. IV), yielding a high local density of states at E_F. The analysis of the 3*s* line in AlMn is complicated by the Al loss structure. Figure 7 shows the spectrum of a 30 percent AlMn alloy in the region of interest and one can see that the surface plasmon of the Al 2*p* line coincides with the Mn 3*s* line at 83 eV. Consequently the plasmon structure of the Al 2*s* line was subtracted from this spectrum in order to display the Mn 3*s* line clearly. Figure 8 shows the Mn 3*s* line obtained in this way for $AlMn_{0.068}$, $AlMn_{0.15}$ and $AlMn_{0.30}$. In all spectra the 3*s* splitting is visible; an analysis of the spectra yields a splitting of 2.9 eV, as compared to 4.3 eV in Mn metal [29] and 6.6 eV in MnF_2 (30). This splitting is a further proof of the magnetic nature of AlMn. A magnetic moment on the Mn ion may only be present, however, on the time scale of the XPS measurement of 10^{-15} s. Thus if we attribute the 6.6 eV splitting in FMn_2 to a moment of $5\,\mu_B$, then the 2.9 eV splitting in AlMn would indicate a moment of $2.2\,\mu_B$ per Mn ion in the alloy. This is a very large value in view of the fact that only an enhanced Pauli paramagnetic susceptibility has been observed in susceptibility experiments [31].

The latter result is probably due to the high spin fluctuation temperature around 500 K. However the

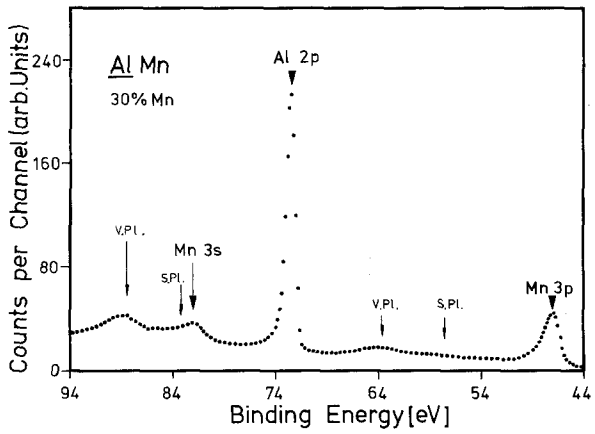

Fig. 7. XPS spectrum of the Al $2p$ and Mn $3p$ and $3s$ region in an AlMn alloy. *v.pl.* indicates the positions of the different volume plasmon lines and *s.pl.* the surface plasmon lines

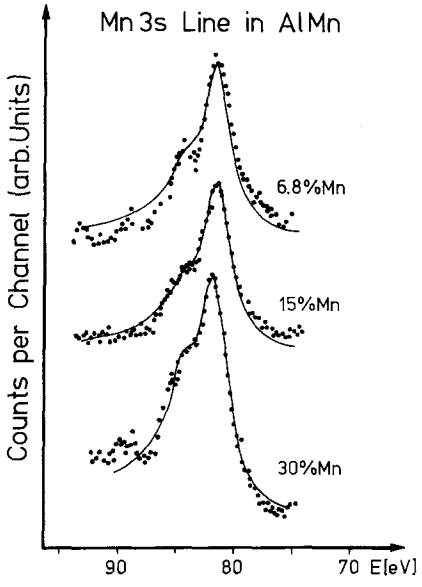

Fig. 8. XPS spectra of the Mn $3s$ region in several AlMn alloys after subtracting the background resulting from the plasmons (see Fig. 7) accompanying the Al $2p$ line. The solid lines through the data points are results of a fit with two lines

depression of the superconducting transition temperature could be explained with a moment of 5 μ_B using a spin fluctuation theory [32]. Thus the moment obtained in the XPS experiments does not contradict either of the other experimental results, because each of them has been performed on a different time scale. It is interesting, however, that by the XPS technique the moment can be directly measured.

IV. Valence Band Spectra

Since the systems investigated here are nonmagnetic (with the exception of AlMn, which is spinfluctuating) we can safely analyse the valence band spectra by the vbs model. For small concentrations this would mean that a symmetrical peak is superimposed on the Al valence band density of states. There will be of course some hybridization and in fact a smearing out of sharp features in the Al density of states by alloying have been observed by Beaglehole and Wihl [9], but for the accuracy of the present data this can be neglected.

In order to analyse the data we have therefore tried to fit them by a superposition of an Al valence band and a line having a Mahan Doniach Sunjić line shape [14], where the asymmetry parameter α is the same as for the corresponding $2p$ core lines and its width and position are to be determined. In order to facilitate this procedure the experimental Al spectrum was converted to a smoothed curve, which is shown in Fig. 9. Figure 9 shows also the valence band alloy spectra analysed in the manner described above and one can see that the data are well represented by the approach chosen.

The parameters extracted from the data analysis are given in Table 1. We note that for Mn, Ni and Cu impurities a number of samples were analysed but for Fe and Co only two were used and so the latter data are less reliable.

The energy of the vbs as a function of d-shell occupancy is shown in Fig. 10. It shows the expected behavior, namely that with increasing number of d-electrons the separation from the Fermi energy increases. Extrapolation of the data shows that the vbs would directly intersect the Fermi energy at Cr as expected from resistivity data and from theoretical calculations.

The values for the width of the vbs in Table 1 contain a contribution from the lifetime of the photohole as well as the contribution from the interaction of the vbs with the conduction electrons. The values in Table 1 can therefore only be regarded as an upper limit for the ground state width of the vbs. The values obtained for AlFe and AlCu are in good agreement with those determined from the depression of the superconducting transition temperature [32]. They are, however, larger than the effective widths of about 0.4 eV obtained by analysing transport data [31]. The vbs in AlCu is slightly narrower and at a slightly lower energy than in $CuAl_2$ [33], a consequence of the higher Al concentration. The same is true in a comparison of the data in AlNi and the AlNi intermetallic compound [34]. The values of the vbs parameters presented in Table 1 are in reasonable agreement with recent theoretical calculations on the basis of scattering theory [35]. Again within this framework and using only d wave scattering the occupancy of the d shell can be calculated from the

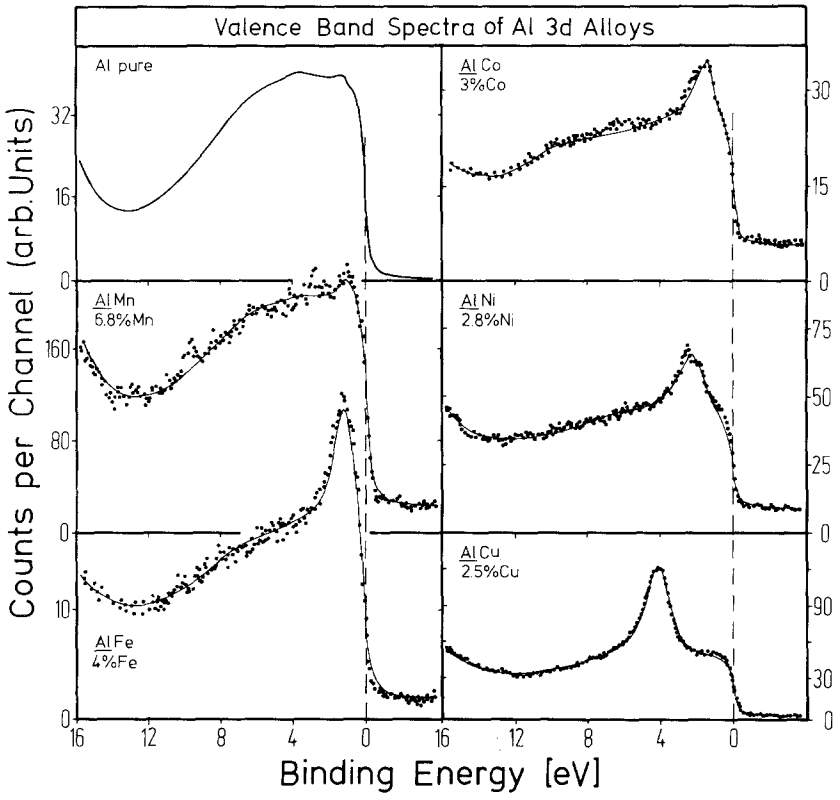

Fig. 9. XPS valence band spectra of Al and Al 3*d* alloys. The solid lines through the data points are results of a fit including a contribution from the valence band of pure Al and a contribution of a virtual bound state from the 3*d* impurity

Table 1. Virtual bound state parameters for 3*d* ions in Al

Ion	E_d (eV)	2Δ (eV)	n_d	$E(2p_{3/2})$ (eV)	ϕ (eV)	ΔE (eV)
Mn	0.7(2)	1.4(3)	7.5(6)	638.7(1)	3.8	0.4(1)
Fe	0.9(3)	1.5(4)	7.8(7)	707.0(2)	4.3	−0.2(2)
Co	1.5(3)	1.6(4)	8.4(4)	778.4(2)	4.4	−0.2(2)
Ni	2.4(2)	1.2(2)	9.2(2)	853.7(1)	4.5	0.2(1)
Cu	4.5(2)	1.1(2)	9.6(1)	933.7(1)	4.4	0.7(1)

ϕ(Al) = 4.25 eV
Numbers given in parentheses represent the experimental errors for the last significant figures.
E_d = position of the vbs relative to E_F
2Δ = full width at half maximum of the vbs
n_d = occupancy of the vbs calculated with Eq. (4)
$E(2p_{3/2})$ = binding of the $2p_{3/2}$ core line of the 3*d* impurity in Al.
ϕ = work function of the pure elements [13]
ΔE = chemical shift of the $2p_{3/2}$ core lines of the 3*d* impurity in Al relative to the pure 3*d* metals.

relation [2]

$$n_d = \frac{10}{\pi} \operatorname{arc\,ctg}\left\{\frac{-E_d}{\Delta}\right\}. \tag{4}$$

These numbers are also given in Table 1. The error bars are large for Mn and Fe. Except for Mn these numbers are in agreement with the assumption, substantiated by various experimental findings, that for Al 3*d* alloys the 3*d* impurity has $(n-1)$ 3*d* electrons, where n is the number of electrons introduced by the 3*d* impurity into the conduction band of Al. Except for Cu these numbers indicate a charge transfer of one electron to the impurity *d*-shell when compared to the pure elements. Table 1 lists also the binding energy $E(2p_{3/2})$ of the impurity $2p_{3/2}$ core lines in the Al host and their shifts ΔE relative to the pure 3*d* metal after a correction for the corresponding work function [13]. Since the relaxation energies due to the screening of the photohole by the conduction electrons should be similar for the Al alloys and the corresponding pure 3*d* metal (a difference of less than 1 eV) these numbers may stand for the chemical shift of the core lines. From a comparison of ionic compounds one expects a shift [36] of about −2 eV for the addition of one 3*d* electron. Therefore the shifts ΔE in Table 1 would only indicate a small 3*d* charge transfer not compatible with the 3*d* occupation of Mn, Fe and Co calculated from the parameters of the vbs with (4). Even in the case of AlNi one expects $n_d = 10$ from the analysis of the core line satellite spectrum and the core line asymmetry, as explained in the previous section. These findings may give a hint that *s* and *p* wave scattering should not be neglected in the analysis of the vbs parameters. The concentration dependence of the vbs intensity has been studied for AlMn, AlNi and AlCu alloys and is shown in Fig. 11

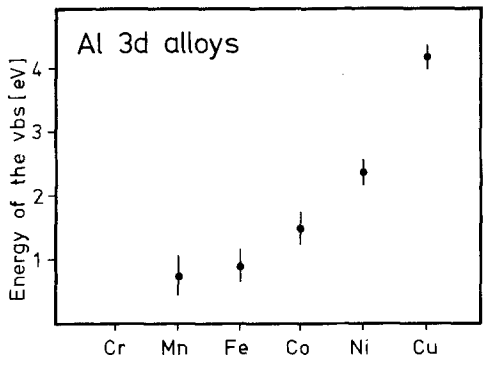

Fig. 10. The position of the virtual bound state of 3*d* impurities in Al relative to the Fermi energy as function of the atomic number of the 3*d* element

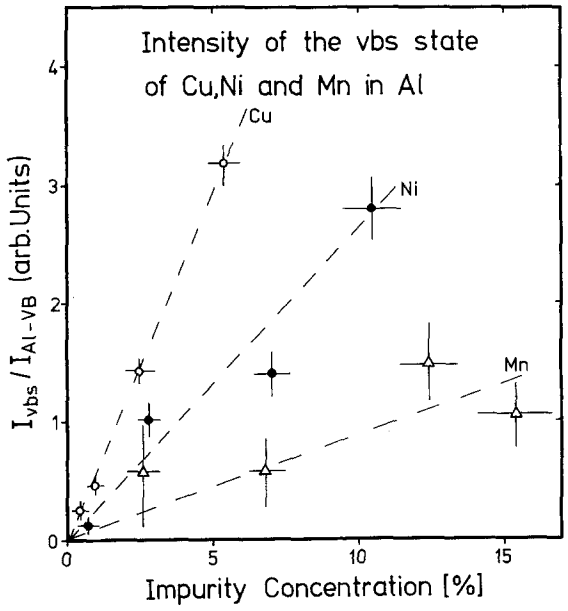

Fig. 11. Concentration dependence of the intensity of the virtual bound state of AlCu (○), AlNi (●) and AlMn (△) alloys normalized to the intensity of the contribution from the Al valence band

normalized to the Al valence band as function of the impurity concentration. Within the experimental accuracy the vbs intensity increases linearly with concentration as expected. The increasing slope of the concentration dependence when going from Mn to Cu reflects the increasing *d*-occupancy of the vbs peak. The slope also depends on the photoabsorption cross section of the *d*-electrons and since these are not known for valence band electrons due to the strong dependence of the photoabsorption cross section on the extent of the corresponding wave functions, it is at present impossible to extract quantitative conclusions from this behaviour.

AlMn is a spin fluctuation system [31]. Accepting the vbs model of Anderson, the measured width Δ can be used to extract U, the effective exchange energy, via $U \simeq \pi\Delta = 2$ eV. This value for U is in good agreement with $U \simeq 1.8$ eV estimated for Ni metal by Herring [37] using various procedures.

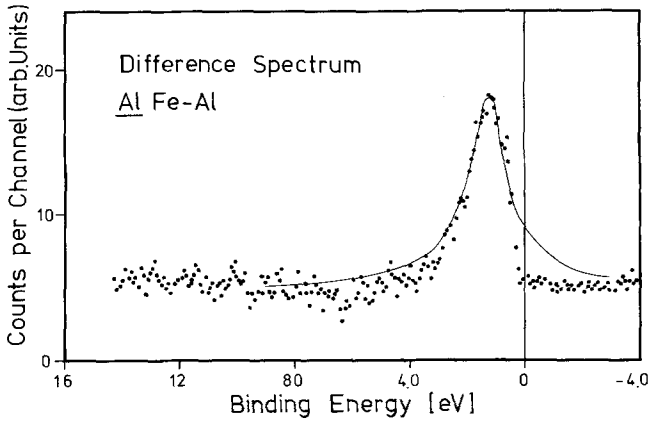

Fig. 12. Difference spectrum of the valence band spectra of AlFe and Al metal. The solid line is the virtual bound state density of Fe as calculated by Anderson and McMillan [38] from *d*-wave phase shifts

It is of interest to see how the investigation of a dilute ("single") impurity of a *d* metal ion can be of use for the understanding of the electronic structure of *d* metals. A possible connection between the two problems comes from the use of scattering theory. The Friedel [1] vbs picture is essentially a scattering theory where the *d* resonance is placed in the *s-p* band of the host metal. Scattering theory has on the other hand been used to treat the electronic states of liquid metals. Anderson and McMillan [38] have employed it to estimate the importance of *d-d* overlap as compared to scattering broadening of the bandwidth of transition metals. They have worked out the case of Fe where they calculated the $l=1$ phase shift for the potential which Mattheiss used for his APW calculation of the band structure of iron. The resonance in the *s-p* band of Fe they obtained by this calculation is shown in Fig. 11, superimposed on the measured vbs of AlFe, where the Al metal spectrum has been subtracted. There is a surprising agreement between the calculated and experimental curve.

This work was supported by the Deutsche Forschungsgemeinschaft.

References

1. Friedel, J.: Can. J. Phys. **34**, 1190 (1956); J. Phys. Radium **19**, 573 (1958); Suppl. Nuovo Cimento **VII**, 287 (1958)
2. Anderson, P.W.: Phys. Rev. **124**, 41 (1961)
3. Hirst, L.L.: Phys. Kondens. Materie **11**, 255 (1970); Z. Physik **241**, 9 (1971); Adv. Phys. **27**, 231 (1977)
4. Rizzuto, C.: Rep. Progr. Phys. **37**, 147 (1974)

5. Wohlleben, D.K., Coles, B.R., in: Magnetism. Rado, G.T., Suhl, H. (eds.), Vol. **V**, p. 3. New York: Academic 1973; see also for several other review articles on magnetic impurities in metals
6. Johnson, K.H., Vvedensky, D.D., Messmer, R.R.: Phys. Rev. B **19**, 1519 (1979)
7. Steiner, P., Höchst, H., Hüfner, S.: J. Phys. F **7**, L 105 (1977)
8. Höchst, H., Steiner, P., Hüfner, S.: Z. Physik B **38**, 201 (1980)
9. Beaglehole, D., Wihl, W.: J. Phys. F **2**, 43 (1972)
10. Myers, H.P., Walldén, L., Karlsson, A.: Philos. Mag. **18**, 725 (1968)
11. Norris, C., Myers, H.P.: J. Phys. F **1**, 62 (1971)
12. Hüfner, S., Wertheim, G.K., Wernick, H.J.: Solid State Commun. **17**, 1585 (1975)
13. Cardona, M., Ley, L.: in Photoemission in Solids I, Topics in Appl. Phys. **26**, 1 (1978); see also for further references
14. Steiner, P., Höchst, H., Hüfner, S.: Z. Physik B **30**, 129 (1978); Photoemission in Solids II, Topics in Applied Physics **27**, 349 (1979); see also for further references on core line shapes in metals
15. Scofield, J.H.: J. Electron Spectr. **8**, 129 (1976)
16. Reilman, R.F., Msezane, A., Manson, A.: J. Electron Spectr. **8**, 389 (1976)
17. Penn, D.R.: J. Electron Spectr. **9**, 29 (1976)
18. Steiner, P., Höchst, H.: Z. Physik B **35**, 51 (1979)
19. Hansen, M.: Constitution of Binary Alloys. New York: McGraw Hill 1958
20. Hüfner, S., Wertheim, G.K.: Phys. Lett. **47** A, 349 (1974), Phys. Lett. **51** A, 299 (1975)
21. Guillot, C., Ballu, Y., Paigné, J., Lecante, J., Jain, K.P., Thiry, P., Pinchaux, R., Pétroff, Y., Falicov, L.M.: Phys. Rev. Lett. **39**, 1632 (1977)
    Penn, D.R.: Phys. Rev. Lett. **42**, 921 (1979)
    Liebsch, A.: Phys. Rev. Lett. **43**, 1431 (1979)
    Tibbelts, G.G., Egelhoff, W.F.: Phys. Rev. Lett. **41**, 188 (1978)
22. Wertheim, G.K., Citrin, P.H. in: Photoemission in Solids **I**, Topics in Applied Physics **26**, 197 (1978); see also for further references
23. Mott, N.F. in: Optical Properties and Electronic Structure of Metals and Alloys, Proceedings of the International Colloquium, Paris, 1965; Abelés, F. (ed.). Amsterdam: North-Holland 1966
24. Kotani, A., Toyozawa, Y.: J. Phys. Soc. Jap. **35**, 1073 (1974) ibid. **35**, 1082 (1973); ibid. **37**, 1073 (1974)
25. Ivan, M., Koch, E.E.: Solid State Commun. **31**, 261 (1979)
26. Fano, U.: Phys. Rev. **124**, 1866 (1961)
27. Ivan, M., Himpsel, F.J., Eastman, D.E.: Phys. Rev. Lett. **43**, 1829 (1979)
    Ivan, M., Koch, E.E., Chiang, T.C., Eastman, D.E., Himpsel, F.J.: Solid State Commun., in press
28. Shirley, D.A. in: Photoemission in Solids I, Topics in Applied Physics **26**, 165 (1978)
29. McFeely, F.R., Kowalczyk, S.P., Ley, L., Shirley, D.A.: Solid State Commun. **15**, 1051 (1974)
30. Kowalczyk, S.P., Ley, L., Pollak, R.A., McFeely, F.R., Shirley, D.A.: Phys. Rev. B **7**, 4009 (1973)
31. Grüner, G.: Adv. Phys. **23**, 941 (1974)
32. Babić, E., Ford, P.J., Rizzuto, C., Salamoni, E.: J. Low Temp. Phys. **8**, 219 (1972)
33. Fuggle, J.C., Watson, L.M., Fabian, D.J., Norris, P.R.: Solid State Commun. **13**, 507 (73)
34. Kowalczyk, S.P., Apai, G., Kaindl, G., McFeely, F.R., Ley, L., Shirley, D.A.: Solid State Commun. **25**, 847 (1978)
35. Dagens, L.: phys. stat. sol. (b) **93**, 279 (1979)
36. Hüfner, S., Wertheim, G.K.: Phys. Rev. B **7**, 5086 (1973)
37. Herring, C. in: Magnetism. Vol. IV. Rado, G.T., Suhl, H. (eds.). New York: Academic 1966
38. Anderson, P.W., McMillan, W.L.: Proceedings of the International School of Physics Enrico Fermi **VII**. Marschall, W. (ed.). p. 50. New York: Academic 1967

P. Steiner
H. Höchst
W. Steffen
S. Hüfner
Fachbereich Physik
Universität des Saarlandes
Im Stadtwald
D-6600 Saarbrücken
Federal Republic of Germany